

The complete catalogue of light curves in equal-mass binary microlensing

Christine Liebig,^{1*} Giuseppe D’Ago,^{2,3†} Valerio Bozza,^{2,3‡} Martin Dominik,^{1,4§}

¹*SUPA, School of Physics & Astronomy, North Haugh, University of St Andrews, KY16 9SS, Scotland, UK*

²*Dipartimento di Fisica “E. R. Caianiello”, Università di Salerno, Via Giovanni Paolo II 132, 84084 Fisciano (SA), Italy*

³*Istituto Nazionale di Fisica Nucleare, Sezione di Napoli, Italy*

⁴*Royal Society University Research Fellow*

Accepted, 30 March 2015. Received, 12 March 2015; in original form, 23 December 2014.

ABSTRACT

The light curves observed in microlensing events due to binary lenses span an extremely wide variety of forms, characterised by U-shaped caustic crossings and/or additional smoother peaks. However, all peaks of the binary-lens light curve can be traced back to features of caustics of the lens system. Moreover, all peaks can be categorised as one of only four types (cusp-grazing, cusp-crossing, fold-crossing or fold-grazing). This enables us to present the first complete map of the parameter space of the equal-mass case by identifying regions in which light curves feature the same number and nature of peaks. We find that the total number of morphologies that can be obtained is 73 out of 232 different regions. The partition of the parameter space so-obtained provides a new key to optimise modelling of observed events through a clever choice of initial conditions for fitting algorithms.

Key words: Gravitational lensing; micro – methods: numerical

1 INTRODUCTION

Einstein (1936) showed that the light curve of a source microlensed by a single foreground compact object is given by an extremely simple symmetric bell-shape, described analytically by a very compact formula, now known as Paczyński curve (Paczynski 1986). It is somewhat frustrating that by adding just another lens the complexity of microlensing explodes so dramatically that after almost 30 years of active theoretical and observational research a complete classification of all possible light curve morphologies is still missing even in the simplest static case! The lack of a complete knowledge of the light curve zoology represents a considerable handicap in the modelling of real microlensing events. In fact, in order to set initial conditions for fitting, one may follow two routes: either blindly set-up a dense grid in the parameter space or identify good initial seeds with light curve morphologies close to the one we wish to model. The first approach is more systematic but can be time consuming and redundant; furthermore, it does not guarantee the completeness of the exploration of all possible corners, which may remain hidden in the space between consecutive points in the grid. The second approach promises to be more efficient in terms of computing time but needs to be supported by a robust and rigorous theoretical framework in order to be safely pursued.

Historically, it is not uncommon for modellers to explore specific morphological traits of light curves to narrow down the parameter space to be searched, as has been done by authors such as Mao & Di Stefano (1995); Dominik & Hirshfeld (1996); Di Stefano & Perna (1997); Albrow et al. (1999a); Dominik (1999a); Han & Gaudi (2008), but literature that systematically covers the whole range of possible morphologies is more scarce. The modelling of observed multiple-lens microlensing light curves requires extensive computation of the magnification curves. Much effort has been invested into speeding up the modelling process, by improving the parametrisation (An et al. 2002; Cassan 2008; Bennett 2010; Bennett et al. 2012; Penny 2014), by employing neural networks to map light curve features to model light curves (Vermaak 2007). Of course this development happened alongside of substantial advances in the code implementation of existing algorithms.

Mao & Di Stefano (1995) discussed a new method for modelling binary microlensing events: the positions and amplitudes of binary light curve extrema are compared to those stored in a pre-compiled (unblended, point-source) light curve library to find promising candidate events, which in turn provide initial parameter sets for a more conventional fitting procedure. This approach works well for multi-peak events, where the source trajectory passes over or close to the binary caustics.

Di Stefano & Perna (1997) developed the library approach further by describing any binary-lens light curve by the set of coefficients of Chebyshev basis polynomials. They note that the Chebyshev expansion will never exactly match the microlensing light curve, because there will be extra extrema and inflection points, but

* cliebig@ari.uni-heidelberg.de

† gdago@unisa.it

‡ valboz@sa.infn.it

§ md35@st-andrews.ac.uk

an arbitrarily precise agreement can be achieved (limited by computational power) by further expansion. In this way, a model search can be refined until the photometric precision of the data points is matched. They find model parameter solutions to *smooth* and *caustic-crossing* light curves by comparing the rough characteristics of the light curve (positions of extrema and inflection points and the magnification values at these points) with a pre-computed light curve library and then searching the nearby environment in the physical parameter space with an increased sampling density until they find a match (or multiple matches) that satisfies the desired precision. In principle, this method is quite good at finding degenerate solutions and higher-order or even non-microlensing parameters can easily be integrated, but again it remains unclear whether all relevant parameter-space regions have corresponding entries in the library. The optimistic assertion that the “morphological features change in a way that is gradual and consistent as the physical parameters are changed” (Di Stefano & Perna 1997) is most likely true for smooth light curves, but for caustic-crossing light curves, we know that very small changes in the source trajectory can have dramatic implications for the number of extrema and their relative positions.

Night, Di Stefano & Schwamb (2008) make a broad distinction between *smooth* light curves and *caustic-crossing* light curves, but the classification is not based on the light curve itself, but on the source trajectory and its closeness to the caustics, i.e. the known simulation parameters, not the observable data. They come to the conclusion that the ratio of smoothly-perturbed to caustic-crossing binary-lens light curves is rather low in survey detections, which can partly be explained by the fact that caustic-crossing peaks stand out unambiguously, whereas smooth perturbations often can have a range of competing explanations (such as binary sources, parallax effects, orbital motion).

In Bozza et al. (2012), a detailed morphological assessment is used for the modelling of OGLE-2008-BLG-510 and furthermore the groundwork is laid for a real-time binary event modelling code (further based on Bozza (2001) and Bozza (2010)). The code relies on a wide choice of starting conditions (“seeds”) from where a search for *local* χ^2 minima is carried out. The choice of seeds is based on the morphology of the binary caustics, with the assumption that binary-lens light curves sampled from a given region of the parameter space lie on a smooth slope of the χ^2 landscape *as long as the morphology of the light curves does not change*. The *morphology* is understood, in this case, as a given peak sequence of caustic crossings and grazings, with any newly created or destroyed peak leading to a change in morphology.

Our intention, with the present work, is to take the move from the path traced by Mao & Di Stefano (1995) and Di Stefano & Perna (1997) and achieve the first complete classification of light curves in the binary microlensing problem. By studying peak-number plots, we can separate groupings of light curves in the binary-lens parameter space. We are not concerned with directly establishing light curve models, but we want to ensure that we classify all possible light curves. We then want to improve our understanding of the relations between the parameter space and the light curves.

The variety of microlensing light curves can seem overwhelming, but the trained eye recognises familiar patterns and translates them back to the parameter space. In fact, the shape of a microlensing light curve does follow certain rules: not any arbitrary curve can be interpreted as a microlensing light curve. Specifically, the limited topologies of the binary lens magnification maps allow only for a limited range of light curve morphologies.

Consequently, the fundamental idea of this work is to identify the building blocks of microlensing light curves and develop a classification scheme that can be directly applied to observed light curves and that allows for a significant narrowing of the modelling parameter space, while, unlike any other approach, guaranteeing completeness. We want to gain a good understanding of the range of possible light curves and how the identified morphological classes relate to subspaces of the modelling parameter space. As a first step, we focus on an in-depth study of the equal-mass binary lens, while the framework developed applies to the general case. On reviewing the properties of this special case in Sec. 2, we use the opportunity to introduce a convenient notation for caustic elements. Sec. 3 introduces our morphology classification scheme, which is based on the four fundamental peak types that occur in microlensing; we also discuss the practicalities, such as the light curve simulation, the peak counting and the identification of iso-maxima regions with light curve morphologies. In Sec. 4, we summarise and discuss the current results of this study, we leave some further considerations to Sec. 5, and stress its future potential in Sec. 6, while the bulk of the content is shown in tabular and graphical form in Table 3 and in Figures 11 to 18.

2 MICROLENSING OF EQUAL-MASS BINARY SYSTEMS

2.1 Parametrisation

Gravitational microlensing is characterised by the angular Einstein radius

$$\theta_E = \sqrt{\frac{4GM}{c^2} \frac{D_S - D_L}{D_L D_S}}, \quad (1)$$

where M is the total mass of the (foreground) lens object, while D_L and D_S denote the lens and source distances from the observer. In the course of a microlensing event, the separation between each pair of images is of the order of θ_E , which is less than a milliarcsecond for typical observed events with the source in the bulge ($D_S \sim 8$ kpc), and the lens being a main sequence star half-way to the source ($D_L \sim 4$ kpc, $M \sim 0.3M_\odot$)

If one assumes uniform, rectilinear relative proper motion μ between the lens and source, the magnification due to a single point lens is described by only three parameters: u_0 , the closest angular impact of the source to the centre of mass expressed in units of θ_E , the Einstein radius crossing time $t_E \equiv \theta_E/\mu$, and the time of closest approach t_0 of the source to the centre of mass of the lens system, which is typically used to fix the epoch of observations, but is irrelevant for the light curve shape. Beyond the single lens parameters, we need the binary mass ratio $q = m_2/m_1$, where m_1 is the primary mass of the binary lens system and m_2 the secondary mass in units of the total mass of the system M , the angular separation of the binary components s in units of θ_E , the angular source star radius ρ still in units of θ_E , and the angle α , between the direction vector from the primary to the secondary and the direction of the source relative to the lens, see also Fig. 1. We assume uniform, rectilinear relative proper motion between source and lens for the simulations and ignore higher-order effects. The observed light curve is the sum of the source flux F_S , amplified by the microlensing effect $A(t; u_0, t_E, t_0, q, s, \rho, \alpha)$, and the blend flux F_B contributed by unresolved sources

$$F(t) = F_S A(t) + F_B. \quad (2)$$

For the purposes of this morphological study, F_S and F_B have no

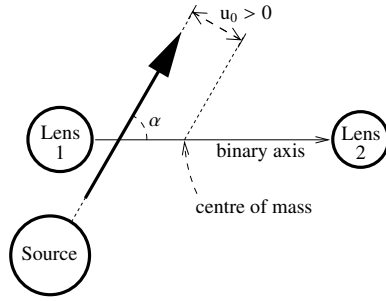


Figure 1. Our definition of u_0 and α . The impact parameter u_0 is positive, when source and lens (centre of mass) pass each other on the right-hand side as projected on the plane of sky. α is the angle between the binary axis (pointing from primary to secondary mass) and the source trajectory.

impact as they just represent a multiplicative and an additive factor respectively.

Our parametrisation is equivalent to the convention detailed in Skowron et al. (2011, Appendix A), except that we regard the source rather than the lens system as moving, resulting in a difference of $\alpha^{\text{here}} = \alpha_0^{\text{Skowron}} - \pi$. A change by π just means the source is travelling in the opposite direction on the same trajectory which does not affect the morphology of the light curve, in other words it is a time reversal of the light curve. More on the parameter space symmetries in Sec. 3.3.

2.2 Caustics

In the theoretical treatment of multiple lens systems, caustics are singular lines where the flux of a point source is infinitely magnified. Schneider & Weiß (1986) have shown that there are exactly three distinct caustic topologies for the case of an equal-mass binary lens. Erdl & Schneider (1993) confirmed this to be true for arbitrary mass ratios. They also noted the transition points in the binary lens separation where the caustic topology changes depending on the lens mass ratio q (also cf. Dominik (1999b)). A caustic enters the *close-separation* topology domain when $s < s_c$,

$$m_1 m_2 = \frac{1}{s_c^8} \left(\frac{1 - s_c^4}{3} \right)^3 \quad (3)$$

and will show the *wide-separation* topology when $s_w < s$,

$$s_w^2 = \left(\sqrt[3]{m_1} + \sqrt[3]{m_2} \right)^3, \quad (4)$$

The three topologies (close, intermediate, wide) are shown in Figs. 2-4 for representative choices of the separation parameter. These figures also contain the labels of the notation to be introduced and discussed in Section 2.3. An isolated pair of lenses close to each other (i.e. $s < \sqrt{2}/2$ for $q = 1$) result in three caustics (Fig. 2): one diamond shaped at the centre of mass, and two small, triangular, secondary caustics set off from the binary axis. If the angular separation of the two lenses is of the order of one Einstein radius, there will be only one central, relatively large, six-cusped caustic, see Fig. 3. For the equal-mass binary lens “of the order of” means the exact range $\sqrt{2}/2 < s < 2$. If the two lenses are far from each other ($s > 2$), two diamond shaped caustics close to the true position of the lenses result. We recollect that caustic lines are always concave in the coplanar binary lens case relevant for Galactic microlensing applications. Petters, Levine & Wambsganss (2001) go into more mathematical detail in describing caustics through singularity theory of differentiable maps.

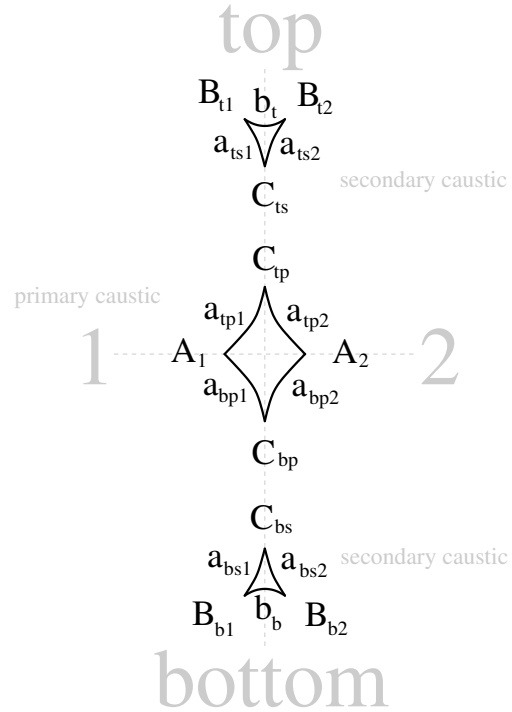


Figure 2. Caustic feature notation of the close-separation binary lens.

Moving from point to extended sources, the singularities of the lens map are regularised by an integration over the finite angular disk of the source. As Schneider & Weiß (1986, Fig. 9) have shown, an increase in angular source size leads to decreased peak magnification, a broadening of the peak width and a displacement of the peak, which means that the maximum will occur later when a larger source enters a caustic (and earlier at the exit). Magnification maps of extended sources feature closed high-magnification lines that can be easily recognised as originating from the smoothing-out of caustics. These high magnification lines asymptotically approach the mathematical caustics as the source size shrinks to zero.

As an aside, introducing a third lens can lead to exceedingly more complicated caustic structures (Rhie 2002). Daněk & Heyrovský (2015b,a) have set out to explore the full range of triple-lens caustic topologies. To quote just one very specific example, the case of three masses positioned at the tips of an equilateral triangle with two equal masses at $(1-\mu)/2$ and a third mass at μ , boasts 10 different caustic topologies. Many of those can be found in other triple-lens scenarios, but the list of ten is nowhere close to covering the whole range possible.

2.3 Notation for caustic elements

All extrema of a binary-lens light curve can be traced back to features of the caustic of the lens system. We have developed a “short-hand” notation for these features, sketched in Figures 2, 3 and 4 and listed in Table 1. In this study, we use and depict this shorthand only for the equal-mass binary lens, but we point out its universal applicability to binary-lens caustics of any mass ratio.

We denote folds of a caustic with a lower-case letter and cusps with an upper-case letter. Local maxima arise either when the source trajectory approaches or crosses a fold or a cusp. We discuss the peak types in detail in Sec. 3.1.

We recall that the magnification of a point source diverges as

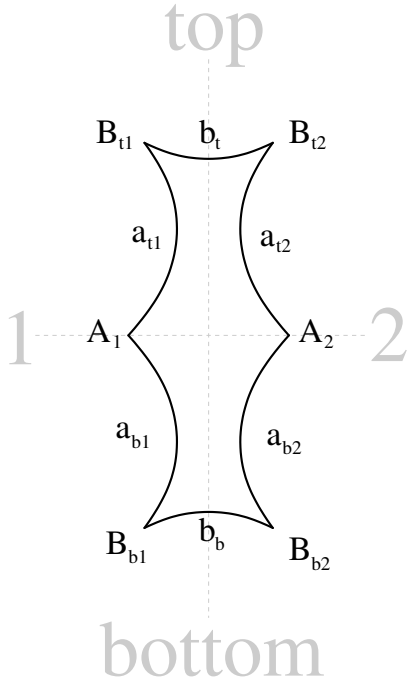


Figure 3. Caustic feature notation of the intermediate-separation binary lens.

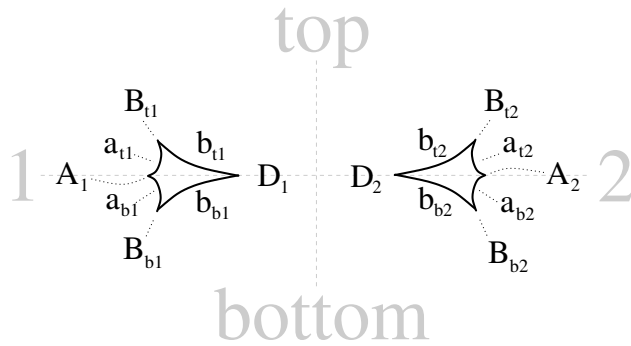


Figure 4. Caustic feature notation of the wide-separation binary lens.

$f_{c,on}/\delta y$ if one hits the cusp along its axis and as $f_{c,off}/\delta y^{2/3}$ if one hits it off-axis (Schneider, Ehlers & Falco 1992). For fold crossing, the magnification diverges as $f_t/\delta y^{1/2}$ when approaching the singular line from the inside. Following these basic analytic formulae, all cusps are strongly magnifying compared to their immediate surroundings. The strength of magnification varies considerably between one point on a fold line and another depending on the factor f_t , which becomes weaker as we move off the binary lens axis.

It is the cusps closest to the binary axis that are the strongest in comparison. In the equal-mass binary case, regardless of the specific topology, the points of maximum magnification are the two “A”-cusps on the binary axis, followed by those parts of the “a”-folds closest to the axis.

The four off-axis cusps (“B”) in the intermediate case, cf. Fig. 3, can be traced across different separations. When the two lenses are moved closer together, the a-folds will eventually merge and split the single caustic line into three separate caustics. The newly created cusps are denoted by “C”. A similar metamorphosis

Notation	Meaning
a, b	fold
A, B, C, D	cusp
1	nearer binary mass 1
2	nearer binary mass 2
t	“above” binary axis (i.e. left of binary vector)
b	“below” binary axis (i.e. right of binary vector)
p	primary caustic (in close-separation case)
s	secondary caustic (in close-separation case)
[a... ; [A...]	caustic entry (via fold; via cusp)
... a] ; ... A]	caustic exit (via fold; via cusp)
[... a ...]	fold grazing (always inside (or on) caustic for binary case)
... A ...	cusp grazing (always outside (or on) caustic for binary case)

Table 1. Caustic feature notation, also illustrated in the sketches in Figures 2, 3 and 4.

takes place, when the two lenses are set further apart, except that in this case the “b”-folds will merge to form the new “D”-cusps.

In the close topology, the closer the two lenses are positioned, the further the two triangular, secondary caustics will move out from the axis and they will continually decrease in size and strength, whereas the central caustic only decreases in size but gains in strength, until the binary lens becomes indistinguishable from a single lens for $s \rightarrow 0$.

Conversely, in the wide topology, the two arrow-shaped caustics become more and more symmetric towards a diamond shape and decrease in size, until for $s \rightarrow \infty$ the B-cusps point perpendicular to the axis and the D-cusps become more equal in strength to the A-cusps. Ultimately the two caustics shrink to two points, at which stage two independent single lenses will be observed rather than one binary system.

All peaks arising from features closer to or facing the lens on the left side are furnished with an index “1”, whereas those nearer the right side lens are indexed “2”. We also want to distinguish the symmetric caustic features, which are mirrored across the binary axis. Quite arbitrarily, we denote them with “t” or top, if they are on the left-hand side of the binary axis (looking from primary to secondary) and “b” or bottom, if they lie on the right-hand side. Figures 2, 3 and 4 better illustrate the “logic” behind this choice.

In the special case of an equal-mass binary under examination, we have a second symmetry axis through the centre of mass, i.e. through the midpoint between the two lenses and perpendicular to the binary axis. This does not affect the choice of notation. The chosen caustic feature notation scheme covers *all* scenarios with two point lenses, including mass ratios very different from unity. The notation scheme is summarised in Table 1.

3 CLASSIFICATION SCHEME AND METHODOLOGY

Having revisited the basic structure of equal-mass binary lenses and having established an alphanumeric notation to identify every fold and cusp in each of the three topologies, we now move to the classification of microlensing light curves. First, we define a light curve morphology based solely on observable features of light curves (Section 3.1). By spanning the whole parameter space of binary microlensing, we simulate light curves (Section 3.2) and assign them to the corresponding morphology class. In this way, we can identify every region in the parameter space in which the same morphology arises as the result of the encounter of a determinate sequence of caustic features by the source along its trajectory (Section 3.3).

3.1 The four peak types in microlensing

Given that the most obvious characteristic of microlensing light curves is the sequence and shape of their local extrema, this sequence provides a natural taxonomic key for our light curve classification scheme. We propose that a class of light curves can be identified by the common sequence of peak types. We then recognise that any microlensing light-curve maximum is created by one of four basic mechanisms. We discuss the four peak types in detail below, but in short summary they are:

- (i) a cusp grazing (\bar{C}),
- (ii) a caustic fold entry (F-) or exit (-F),
- (iii) a cusp entry (C-) or exit (-C),
- (iv) a fold grazing (\bar{F} -).

Now, in detail: (i) the *cusp grazing*, \bar{C} : The peak that arises when the source passes outside the caustic but close enough to one of the cusps to pass over the lobe of increased magnification, is a “cusp grazing”. We unambiguously call a light curve “cusp-grazing”, if the source trajectory is outside the caustic pre and post-peak and only a single peak results. The Paczyński curve can be understood as a grazing of the point caustic (or infinite-order cuspid) of the single lens. The name *Paczyński curve* should be reserved for single lens light curves only, but in the limits where a binary lens resembles a single lens, when the source does not pass close to the caustics or when the caustics are very small relative to the solid angle of the source, a single-peaked light curve will result. We do not register any morphological difference to the cusp grazing in the narrow sense.

(ii) the *fold entry/exit*, F-/F: When the source enters on a caustic fold, this creates a very distinctly shaped curve (cf. Schneider, Ehlers & Falco (1992); Gaudi & Petters (2002)), with a steep, almost vertical rise followed by a more parabolic fall, which does not descend as low as the caustic-exterior magnification. The morphology is mirrored in the fold exit. A pair of fold entry and exit peaks give rise to the familiar *double caustic crossing* signature.

(iii) the *cusp entry/exit*, C-/C: If the caustic is entered or exited along a cusp, the peak will have a more symmetric shape, because the lobe outside the caustic and the close proximity of the fold lines on the inside of the caustic attenuate the gradient of the passage on both sides. The fact that the magnification in the caustic interior is increased can help to distinguish it from a cusp-grazing¹.

(iv) the “interior fold approach” or *fold grazing*, \bar{F} -: This type of peak occurs inside the caustic, while the source trajectory passes close to a caustic fold. Due to the concavity of the caustic lines, the fold-grazing peak will only be observed if it is an *interior* approach. A special case is the peak that occurs when two or more caustic lines are close enough or strong enough to raise the magnification of an extended area between them, giving rise to a peak that cannot be directly attributed to one single fold.

These “building blocks” of microlensing light curves can be sequenced, subject to a few rules:

- a caustic entry must be followed by a caustic exit²
- a caustic exit cannot occur, if the caustic has not been entered before

- a fold grazing can only take place inside a caustic
- a cusp grazing can only take place outside a caustic
- due to the concave curvature, a straight caustic-crossing trajectory must exit by a fold (or cusp) different from the one through which it entered (Cassan et al. 2010)

All binary microlensing light curves (in the parameter space considered in this study) adhere to these rules, but just conforming to these rules does not guarantee a microlensing light curve since the possible caustic topologies are limited (Erdl & Schneider 1993).

It is well known that similar light curve morphologies may arise in completely different situations, with source trajectories interacting with different cusps or folds in different topologies. Such disconnected regions can be identified by specifying the folds and cusps involved using the notation introduced in Sec. 2.3. Then the symbols identifying a sequence of peaks conforming to a specific morphology class (e.g. F-F \bar{C}), can be replaced by the corresponding caustic elements involved (e.g. $[a_1, b_1]B_{12}$). Since the folds and cusp symbols already carry subscripts, in order to generate more reader-friendly sequences, we indicate the caustic entry and exits by square brackets and suppress the bar for the grazings. So a fold entry is “[a...”, a cusp entry “[A...”, with the exit being “...]”. A fold grazing is “[...a...]” and a cusp grazing is given by “A”. These notations detailing the caustic features involved in the light curve morphology sequence are also summarised in Table 1. We will use the synthetic notation (e.g. F-F \bar{C}) for identifying a light curve morphology class irrespective of its possible interpretations in terms of source trajectories and caustics involved, and the detailed notation ($[a_1, b_1]B_{12}$ in this example) to identify the iso-maxima region(s) in the parameter space giving rise to that specific morphology.

To see an example of a light curve classification “at work”, consider the light curve in Fig. 11(h) where we see a (symmetric) cusp entry (C-) paired with an (asymmetric) fold exit (-F) and a post-caustic grazing of the cusp lobe (\bar{C}),

$$\underbrace{C-F}_{\text{caustic traversal}} \underbrace{\bar{C}}_{\text{cusp lobe}}.$$

The detailed sequence specifying the folds and cusps involved in this light curve is $[A_1 a_{12}]A_2$.

Fig. 12(d) gives a nice example with a clear-cut fold entry (F-), followed by a second peak still inside the caustic, which can only be an inner fold approach (\bar{F} -), a fold exit (-F) and followed by a final cusp lobe grazing (\bar{C}), so we classify it as

$$\underbrace{F-\bar{F}-F}_{\text{caustic traversal}} \underbrace{\bar{C}}_{\text{cusp lobe}}.$$

The detailed sequence specifying the folds and cusps involved in this light curve is $[a_{b_1} a_{t_1} a_{t_2}]B_{12}$.

Keeping the caustic geometry fixed and displacing the source trajectory, we can appreciate the changes in the light curve morphology, with peaks merging or disappearing while other peaks appear or separate in two. These transition morphologies need some further attention in order to be assigned to specific classes without ambiguities.

In this respect, consider the case of Fig. 5, representing the morphing from two fold crossings F-F to a cusp grazing \bar{C} . When the extended source trajectory cuts a cusp nearly perpendicularly to its axis, the light curve features a transition morphology with a single peak preceded and followed by derivative discontinuities, typical of fold crossings (trajectories ST2 and ST3 in Fig. 5). Introducing a new intermediate “cusp cutting” class would not be very useful, since the detection of the two discontinuities at the base of

¹ Mao, Witt & An (2013) have recently shown that this is not necessarily the case for a multi-planar lens distribution.

² For $n > 3$ lenses the number of entries and exits may be unequal as caustic lines can be intersecting and nesting. For $n = 2$, one caustic entry must be followed by one caustic exit, before another caustic entry can occur.

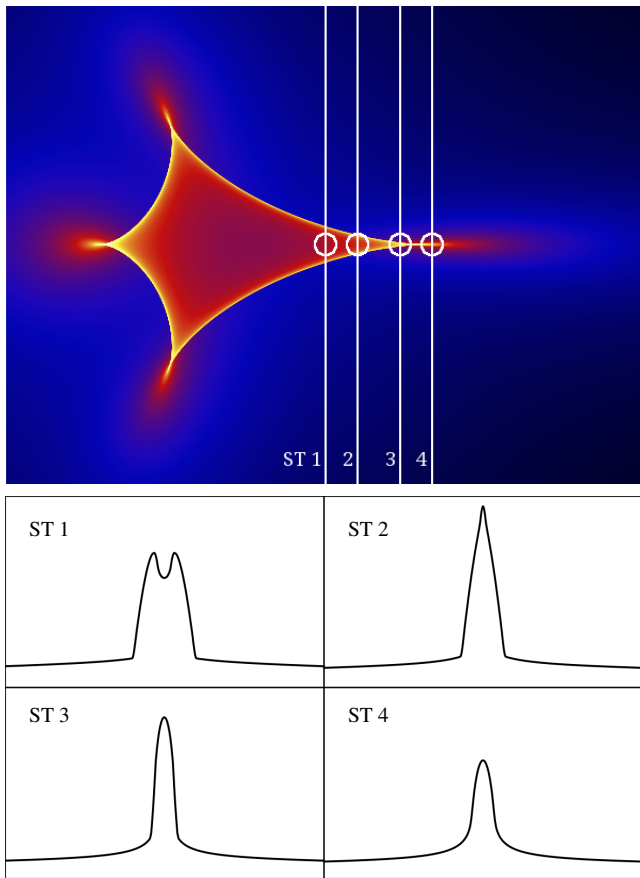


Figure 5. Comparison of *fold-crossing* and *cusp-grazing* source trajectories (ST 1 to 4) and resulting light curves. The angular source size is indicated by the white circles. From left to right, the light curve morphology evolves from a double fold crossing F-F for ST 1 to a cusp grazing \bar{C} (ST 2, 3 and 4). Where exactly this transition occurs depends on the angular source size; with a smaller source, ST 2 would also lead to a double-peaked fold crossing.

the peak could never be unambiguously assessed in real observations. Only a very detailed analysis of the light curve would distinguish a cusp-cutting from a cusp-grazing trajectory. Keeping in mind that the purpose of our study is to identify regions in the parameter space that may give rise to independent seeds for model searches, we assign these cusp-cutting peaks to the broader cusp grazing class, extending its definition by including all trajectories for which the cusp cutting does not give rise to two fold-crossing peaks with a dip in between. In some sense, this statement is already contained in the above definition, in which we required that the source is outside the caustic pre- and post-peak and only one peak occurs. This specific example should help avoiding any confusion.

It follows that the peak classification does not just depend on the source trajectory relative to the lens positions, but equally on the angular source size relative to the caustic size. I.e. a given source trajectory (e.g. ST 2 in Fig. 5) can yield an F-F morphology for a smaller source and a \bar{C} morphology for a larger source, whereas for a given source size ST 1 can result in an F-F pair, but ST 2 will only show a single peak and be classified as cusp-grazing \bar{C} .

Another situation almost complementary to the previous one occurs when a fold grazing morphs into two fold crossings as the source trajectory changes from fully internal to tangent and then

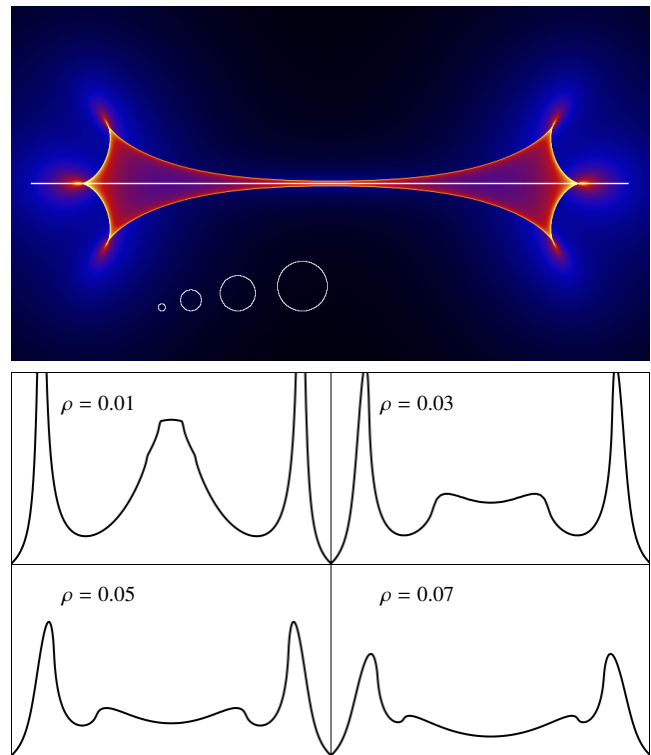


Figure 6. Classification in the case of a beak-to-beak metamorphosis. The magnification curves result from the same source trajectory, but with different source sizes (as indicated by the white circles). The smallest source produces an unambiguous *fold-grazing*, as the central peak occurs inside the caustic (C-F-C). Interestingly, the larger sources create a central pair of peaks instead, thus leading us to classify the light curves as C-C C-C. This might seem counterintuitive, before one considers the convoluted magnification pattern, where it becomes clear that a larger source shifts the position of the beak-to-beak fold merger – thereby causing the caustic topology change to occur at a smaller separation compared to the smaller source.

secant to the fold. Adopting the same convention as before, we extend the “fold grazing” class to include the transition peak occurring when the source moves tangentially to the fold, as long as the peak remains single.

Transition morphologies can be more complicated than these two cases illustrated above and may also involve changes in the caustic topologies. In Fig. 6, we have a fold-grazing source trajectory C- \bar{F} -C, across a caustic that is close to the limits of the intermediate-to-wide transition, which morphs into a cusp exit/entry pair, C-C C-C, with an increased source size.

In summary, all sorts of transitions can be safely treated by adopting the extended definitions of cusp grazing and fold grazing classes just described, including the transition peaks before they split into two. Now we are ready to apply our classification scheme to arbitrarily complicated light curves without facing any more ambiguities.

3.2 Light curve simulation and processing

In order to achieve a complete classification of binary lens light curve morphologies, we process simulated light curves. We then consider light curves grouped in the parameter space by their number of maxima. The parameter space we want to cover is the equal-mass lens ($q = 1$), the separation s across all topologies and the

source trajectory parameters $0 \leq \alpha < 2\pi$ and u_0 as far as new morphologies can be expected to occur. We use an extended source with angular radius $0.002 \theta_E$. For each light curve we record the number of peaks and visualise the results in peak-number plots (over α and u_0). The resulting iso-maxima regions are examined with regard to the contained light curve morphologies. Broadly speaking, an iso-maxima region, covering a “bundle” of neighbouring source trajectories, corresponds to a specific sequence of caustic features. One step up in the classification hierarchy, different iso-maxima regions are collected in morphology classes (as introduced in Sec. 3). The fixed source size used in our investigation is small enough to probe the caustics of an equal-mass binary lens in detail but large enough to let cusp crossings occur in finite regions of the parameter space. Different choices will cause a slight shift of the boundaries of the iso-maxima regions (cf. Figs. 5 and 6). This point is further discussed in Sec. 5.

In our examination of the equal-mass binary lens case, we simulate microlensing light curves for all (relevant) volumes of the (s, α, u_0) parameter space. We simulate the light curves with inverse ray shooting, using a software library written in 2010 by Marnach³. Assuming static lenses, this means we can compute magnification maps for every (q, s) set, fold them with the source star profile with a radius ρ and then extract a large number of light curves differing in α and u_0 at virtually no computational cost. During the peak counting, numerical noise can create artificial peaks and troughs, especially for source trajectories that run at a small angle to fold lines. To avoid these, we require a minimal difference between the maximum and the minima on either side of 5% of the nearest local minimum value, before a trough-peak-trough occurrence is counted as a peak. Because of this threshold, sometimes true peaks will be disregarded in the maxima counting algorithm. But this is unlikely to make us miss a whole iso-maxima region, as generally the region boundary (where the formerly disregarded peak becomes significant) will only be slightly shifted in the (u_0, α) plane.

3.3 Iso-maxima regions

Per examined separation, we plot the number of local maxima per light curve over α , u_0 of its source trajectory, see Fig. 7. In the resulting plot, we can identify and isolate regions of a uniform peak number, which we call *iso-maxima regions*.

Due to the inherent symmetries, we can restrict ourselves to the first quadrant, $0 < u_0, 0 < \alpha < \pi/2$. Beyond the trivial periodicity of α with period 2π , there are several symmetries in the two-dimensional (u_0, α) space. Generally, for a binary lens,

$$(u_0, \alpha) \Leftrightarrow (-u_0, -\alpha) \quad (5)$$

is an exact degeneracy, which is caused by the intrinsic symmetry of the binary lens across the binary axis. Skowron et al. (2009, Appendix A) argues (and this has been common practice for a while, see e.g. Albrow et al. (1999b)) that models for static binaries should be expressed in the range $u \geq 0$ and $0 \leq \alpha < 2\pi$, with the exception of cases that display parallax effect where the apparent source position can appear on both sides of the lens. We generally subscribe to this view, nonetheless it is instructive to, at least once, visualise the “full” parameter space, see Sec. 4.

Since we are interested in the morphology only,

$$(u_0, \alpha) \Leftrightarrow (-u_0, \alpha + \pi), \quad (6)$$

gives the symmetry of a time reversal (where the sign of u_0 has to change according to the convention, because the source now passes the lens on the other side). We can also combine the two,

$$(u_0, \alpha) \Leftrightarrow (u_0, \pi - \alpha). \quad (7)$$

For the special case of the equal-mass binary, we also have a perfect degeneracy

$$u_0 \Leftrightarrow -u_0, \quad (8)$$

i.e. the plot is axis-symmetric in u_0 .

We note that whenever one moves from one iso-maxima region to a neighbouring one, the morphology of the light curve peaks changes – naturally, because the border will be overstepped whenever a peak is created or destroyed. We record the caustic feature sequence for the light curves of each region, see Table 2, and realise that in a given quadrant, there are no two iso-maxima regions with the same number of peaks that contain the same sequence of caustic features.

We then map the caustic features to the broader peak typology, thereby reducing the complexity of the light curve description and enabling us to collate different regions in more general morphology classes.

4 RESULTS

Focussing on the equal-mass binary lens, we analysed peak-number plots spanning all three caustic topologies and the two transitioning cases: close ($s = 0.5, 0.65$), close-to-intermediate ($s = 0.7$), intermediate ($s = 0.85, 1.0, 1.5$), intermediate-to-wide ($s = 2.05$) and wide ($s = 2.5$). As discussed in Sec. 3.2, we were motivated to use an extended source with an angular radius, $\rho = 0.002$ (in units of θ_E) and work with a peak threshold of 5% above the nearest minima.

Within the peak-number plots, we know the light curve composition in each (substantial) iso-maxima region, i.e. we know which sequence of caustic features produces the observable peaks of all light curves in that region. We note that it is mostly a bijective mapping, with only very few regions containing more than one kind of caustic feature sequences. In no case, do two unconnected regions share the same caustic feature sequence.

The light curves (and iso-maxima regions) are collected in morphology classes, where each peak is morphologically classified as one of the following: cusp-grazing, cusp-crossing, fold-crossing or fold-grazing. A substantial subset of morphology classes can be found in all examined separation settings. Other classes only appear when a higher or lower separation leads to multi-caustic topologies, whereas the specific example of a double fold grazing is necessarily limited to the intermediate caustic cases.

The extreme variety of binary microlensing phenomenology can be appreciated by summarising the results of our search in a few numbers. We have found 73 different light curve morphologies according to our classification based on the sequence of peaks. These morphologies arise in 232 independent regions of the parameter space. The simplest morphologies can be obtained in many different ways. For example, the simplest caustic crossing light curve class, F-F, can be found in 7 disconnected volumes of the parameter space. If we add shoulders to this caustic crossing, with the classical sequence \bar{C} F-F \bar{C} , we find 9 different volumes. We emphasise the fact that thanks to our thorough investigation we are able to quantify the exact number of independent physical models that can qualitatively reproduce an observable light curve for the

³ Published at <https://github.com/smarnach/luckyensing>.

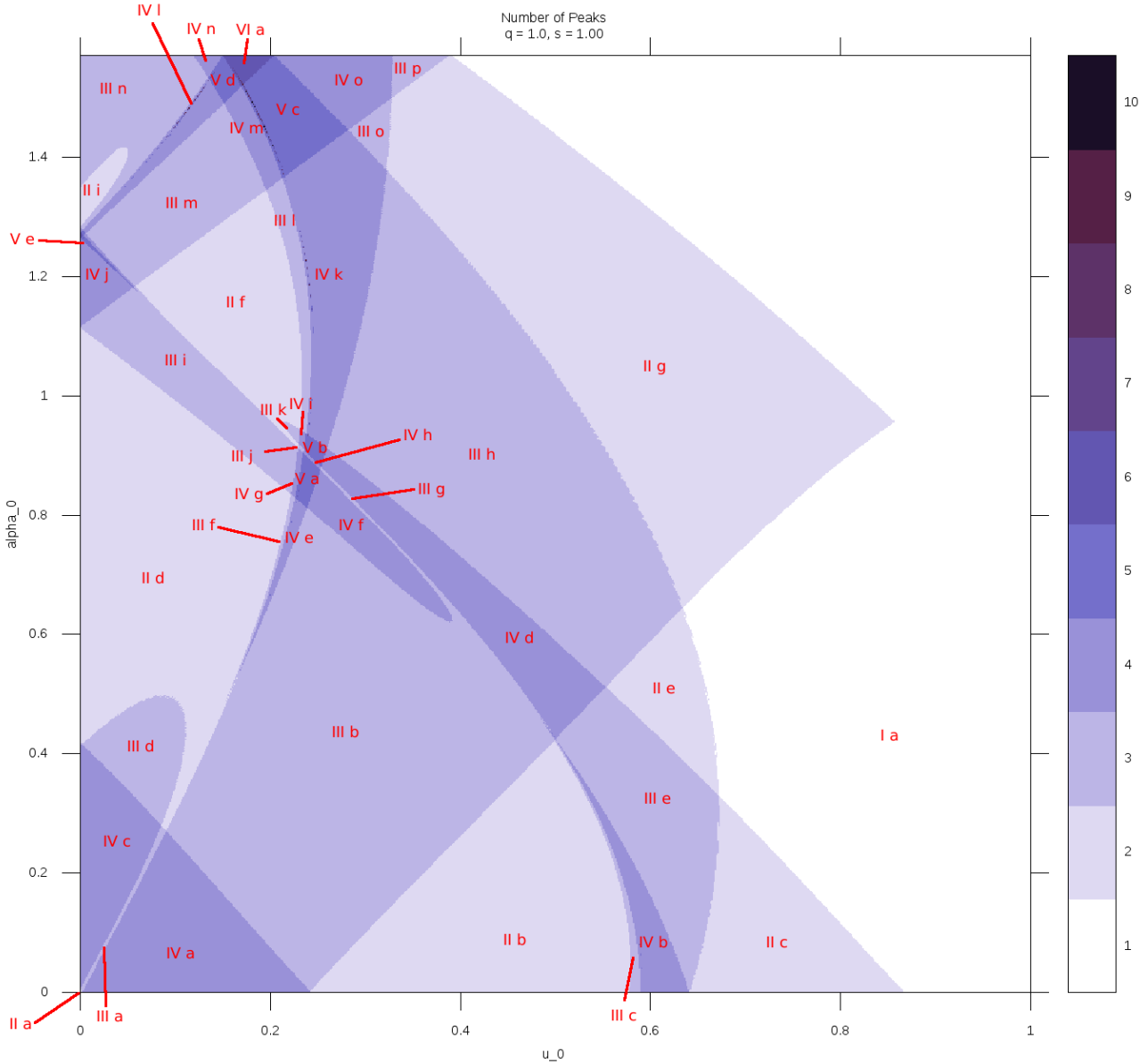


Figure 7. Plot of the number of maxima per light curve in the first quadrant of the (u_0, α) parameter space for the equal-mass binary lens at separation $s = 1.0$ (intermediate caustic topology): *white* means the light curve has a single peak, *dark blue* means six peaks, *higher values* are numerical noise in this instance. Each labelled region represents a grouping of source trajectories and corresponding light curves that follow a specific caustic feature sequence, see Table 2. Rarely are two regions with the same number of peaks directly connected (cf. III b and III g above).

first time! More complicated morphologies with multiple caustic crossings are rarer and appear in fewer regions of the parameter space. A microlensing light curve for an equal-mass binary lens can have up to 10 peaks, if the source moves near the vertical axis of a close configuration.

5 FURTHER CONSIDERATIONS

Source size A hypothetical point source is often useful in theoretical studies of the behaviour of gravitational lenses, but because we want to examine the range of real, observable light curve morphologies, we use an extended source size of $0.002 \theta_E$ for our simulations. The source size does influence the shape of a light curve,

as discussed in Sec. 3. A pair of fold crossings can be merged into a single peak, a whole caustic can be crossed and appear as a single peak, but as long as the solid angle of the source area is small relative to the caustic extent, the absolute size will not change the number of distinct morphologies that can be studied. For the studied mass ratio $q = 1$, we can afford to use a moderately large source that reduces the numerical noise in our samples. Meaningful studies of planetary mass ratios $q \lesssim 10^{-3}$, require a smaller source size. We point out that not all of the peak types of Sec. 3.1 can be simulated with a point source: the cusp crossing can only occur, if the point source enters the caustic *exactly* over the infinitesimal cusp point. The probability for this occurrence is therefore zero.

Two peaks will generally merge into one, if their angular sep-

Region label	Caustic feature sequence	Morphology class
I a	A_1 or B_{11}	\bar{C}
II a	$[A_1 A_2]$	C-C
II b	$[a_{t1} a_{t2}]$	F-F
II c	$B_{t1} B_{t2}$	C-C
II d	$[a_{b1} a_{t2}]$	F-F
II e	$[a_{t1} b_t]$	F-F
II f	$[a_{b1} b_t]$	F-F
II g	$A_1 B_{t1}$	C-C
II h	$[b_b b_t]$	F-F
II i	$[b_b b_t]$	F-F
III a	$[A_1 a_{t2}] A_2$	C-F \bar{C}
III b	$A_1 [a_{t1} a_{t2}]$	\bar{C} F-F
III c	$[a_{t1} b_t a_{t2}]$	F- \bar{F} -F
III d	$A_1 [a_{b1} a_{t2}]$	\bar{C} F-F
III e	$[a_{t1} b_t] B_{t2}$	F-F \bar{C}
III f	$[a_{b1} a_{t1} a_{t2}]$	F- \bar{F} -F
III g	$A_1 [a_{t1} B_{t2}]$	\bar{C} F-C
III h	$A_1 [a_{t1} b_t]$	\bar{C} F-F
III i	$[a_{b1} a_{t2}] B_{t2}$	F-F \bar{C}
III j	$[a_{b1} a_{t1} B_{t2}]$	F- \bar{F} -C
III k	$[a_{b1} b_t] B_{t2}$	F-F \bar{C}
III l	$[a_{b1} a_{t1} b_t]$	F- \bar{F} -F
III m	$B_{b1} [a_{b1} b_t]$	\bar{C} F-F
III n	$[b_b a_{b1} b_t]$	F- \bar{F} -F
III o	$[a_{b1} a_{t1}] B_{t1}$	F-F \bar{C}
III p	$B_{b1} A_1 B_1$	\bar{C} \bar{C} \bar{C}
IV a	$A_1 [a_{t1} a_{t2}] A_2$	\bar{C} F-F \bar{C}
IV b	$[a_{t1} b_t] [b_t a_{t2}]$	F-F F-F
IV c	$A_1 [a_{b1} a_{t2}] A_2$	\bar{C} F-F \bar{C}
IV d	$A_1 [a_{t1} b_t] B_{t2}$	\bar{C} F-F \bar{C}
IV e	$[a_{b1} a_{t1}] [a_{t1} a_{t2}]$	F-F F-F
IV f	$A_1 [a_{t1} a_{t2}] B_{t2}$	\bar{C} F-F \bar{C}
IV g	$[a_{b1} a_{t1} a_{t2}] B_{t2}$	F- \bar{F} -F \bar{C}
IV h	$[a_{b1} a_{t1}] [a_{t1} B_{t2}]$	F-F F-C
IV i	$[a_{b1} a_{t1} b_t] B_{t2}$	F- \bar{F} -F \bar{C}
IV j	$B_{b1} [a_{b1} a_{t2}] B_{t2}$	\bar{C} F-F \bar{C}
IV k	$[a_{b1} a_{t1}] [a_{t1} b_t]$	F-F F-F
IV l	$[b_b a_{b1}] [a_{b1} b_t]$	F-F F-F
IV m	$B_{b1} [a_{b1} a_{t1} b_t]$	\bar{C} F- \bar{F} -F
IV n	$[b_b a_{b1} a_{t1} b_t]$	F- \bar{F} - \bar{F} -F
IV o	$B_{b1} [a_{b1} a_{t1}] B_{t1}$	\bar{C} F- \bar{F} -F
V a	$[a_{b1} a_{t1}] [a_{t1} a_{t2}] B_{t2}$	F-F F-F \bar{C}
V b	$[a_{b1} a_{t1}] [a_{t1} b_t] B_{t2}$	F-F F-F \bar{C}
V c	$B_{b1} [a_{b1} a_{t1}] [a_{t1} b_t]$	\bar{C} F-F F-F
V d	$[b_b a_{b1}] [a_{b1} a_{t1} b_t]$	F-F F- \bar{F} -F
V e	$B_{b1} [a_{b1} a_{t2}] [a_{t2} b_t]$	\bar{C} F-F F-F
VI a	$[b_b a_{b1}] [a_{b1} a_{t1}] [a_{t1} b_t]$	F-F F-F F-F

Table 2. Caustic feature sequences for the iso-maxima regions in Fig. 7 ($q = 1.0$, $s = 1.0$). Each sequence is unique to its region, while the morphology classes generally span several independent regions.

ation is smaller than the angular source diameter (disregarding limb-darkening effects). In our simulations the source has a diameter of $4 \times 10^{-3} \theta_E$, i.e. peaks within $4 \times 10^{-4} t_E$ of each other would be missed. We work with the assumption that a larger source size can only lead to a smaller number of identified morphologies. This has been visually demonstrated for $q = 1.0$, $s = 1.0$ in Fig. 8. Liebig (2014) also documents the entirety of morphological classes for a source radius of $10^{-2} \theta_E$ and they are a subset of the morphology presented here.



Figure 8. Comparison of peak-number plots resulting from different source sizes (from top to bottom: $\rho = 0.005, 0.01, 0.02 \theta_E$), scale and ranges as in Fig. 7: x -axis: $0 \leq u_0 \leq 1.0$, y -axis: $0.0 \leq \alpha \leq \pi/2$. The change in iso-maxima regions is subtle, but noticeable. The smallest source not only leads to more iso-maxima regions, but also to more numerical artefacts. Also compare Fig. 7, where $\rho = 0.002 \theta_E$.

Error margin While we aim for completeness, due to the numerical nature of our study we have to ignore very small sub-regions of the studied parameter space and therefore might have missed out on a particular light curve morphology. Within this space we have examined all iso-maxima regions larger than 10 by 10 pixel, i.e. $10^2 \times 1/(u_0\text{-sampling}) \times \frac{\pi}{2}/(\alpha\text{-sampling})$, meaning that within a given Einstein radius and with our sampling of 1600, the probabil-

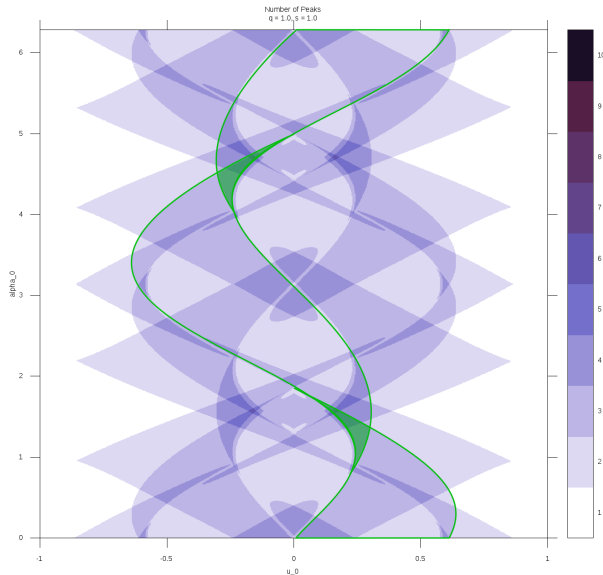


Figure 9. Extended plot of the iso-maxima regions for $s = 1.0$ to illustrate existing symmetries and the seamless continuation of iso-maxima regions beyond the first quadrant. We have marked a caustic feature region: the green outline frames the area where the a_{11} fold gives rise to a light curve peak, more specifically the top and bottom regions contain the fold entry $[a_{11} \dots]$ whereas the middle region contains the fold exit $[\dots a_{11}]$. The green shade marks areas where the a_{11} fold is crossed twice (requiring $[\dots a_{11}][a_{11} \dots]$ to be part of the light curve). Moving to a slightly smaller u_0 from the shaded area, the light curves will display the fold grazing $[\dots a_{11} \dots]$.

ity to observe that particular light curve morphology is smaller than $\leq 1/16000$.

Caustic feature regions It is highly instructive to consider the complete parameter space volume that corresponds to a peak created by a particular caustic feature. This *caustic feature region* will cover several iso-maxima regions, where the light curves show one or two peaks due to this particular caustic element, see an example in Fig. 9. If this information content could be properly harnessed, it would provide an immediate key for the mapping of the lens system to the light curve and from the light curve morphology to the caustic.

For caustic-crossing point sources, this problem often reduces to registering the intersection points of the straight source trajectory with the caustic, which is a mathematically well-defined problem. However, for non-caustic crossing peaks (i.e. cusp and fold approaches), caustic lines do not provide sufficient information. It would be necessary to study the magnification map around caustics in order to pin down the position of the maximum magnification along the source trajectory and then assign this position to a nearby caustic fold or cusp for classification. This approach appears too complex to implement in practice.

6 CONCLUSION AND FUTURE PROSPECTS

We have compiled an unprecedented catalogue of microlensing light curve morphologies for the equal-mass binary lens. We realised that all peaks in microlensing light curves can be classified in just four categories: cusp-grazing, cusp-crossing, fold-crossing

or fold-grazing. In order to achieve this complete classification, we have developed a general notation scheme for the features of binary-lens caustics. Our tool, plots of peak number over u_0 and α , serves to provide insight into the microlensing parameter space.

Before this work, statements of the diversity of binary microlensing light curves were only made on reasonable but vague arguments. With our detailed study we are able to assign numbers to all specific cases and open the way to more quantitative studies of binary microlensing.

Apart from the pure taxonomical aspects, which are very interesting from the theoretical point of view, Table 3 stands out as a very powerful tool for modellers to relate an observed light curve to all possible regions of the parameter space in which this light curve can be found. This capability would help the construction of more fail-safe algorithms that will guarantee a full exploration of the microlensing parameter space. In practice, seeds for fitting algorithms can be placed in the middle of each iso-maxima region so as to ensure a full exploration of all possible cases. Among the currently running platforms for modelling using this principle for setting initial conditions, we mention RTModel (Bozza 2010; Bozza et al. 2012). The inclusion of our catalogue in the template library consulted by RTModel would further diminish the chances of missing any particular region in the parameter space.

Another interesting aspect that can be further investigated is the probability of the occurrence of a given morphology. Having traced the iso-maxima regions in the parameter space, it should not be difficult to translate the volumes of the iso-maxima regions in probabilities normalised by a physically motivated measure. In this way, we would be able to quantify how “rare” or common a morphology is. The current iso-maxima plots would already suffice for probabilities at fixed lens separations. However, for a more complete and useful study, one should move through different lens separations with a much smaller sampling step, so as to characterise the shapes and the volumes of the regions in a more accurate way. Furthermore, the final result would depend on the assumed prior distribution function for the separations of binary systems. Summing up, the study of the relative frequencies of the different morphology classes is certainly one of the most interesting directions opened up by our work, which deserves the greatest attention and an adequate space in dedicated future works.

We have only very briefly mentioned the existence of caustic-feature regions as “meta regions” to the iso-maxima regions, i.e. the combination of all iso-maxima regions containing one specific, caustic-related peak. Unfortunately, we have not yet found a good way to extract and preserve the information about these meta regions, but in fact they can provide a more fundamental understanding of the parameter space, since iso-maxima regions are basically just “stacks” of caustic-feature regions. In contrast to iso-maxima regions, caustic-feature regions are smooth structures and, like the caustics they are derived from, they change continuously over the parameter space. If their boundaries could be analytically derived from the caustic lines, an elegant automatic classification could be achieved.

Finally, we must remember that our work is limited to the equal-mass static lens case. Higher order effect such as parallax and orbital motion would dramatically increase the complexity of the classification, adding very few new morphologies (at least in reasonable physical cases) and would mainly distort existing iso-maxima regions. The only really relevant and humanly achievable upgrade of our catalogue should include a variable mass ratio.

While previous literature has shown only up to three pairs of caustic crossings for a single microlensing caustic (e.g. Cassan

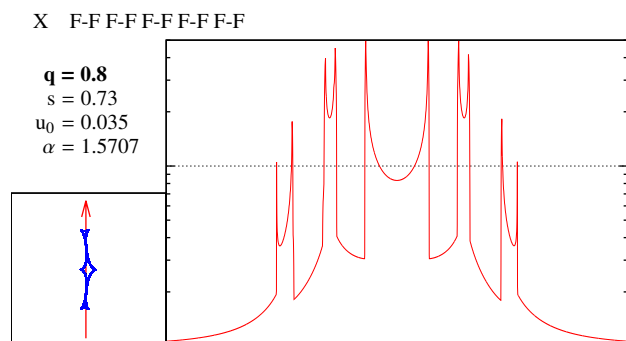


Figure 10. Five pairs of double caustic crossings in one ten-maxima light curve. This “quintuple F-F” morphology cannot be created with an equal-mass binary. The light curve is plotted as magnification on a logarithmic scale in the range from 1 to 50 (dotted line at magnification 10), the time axis covers four Einstein times. The small plot shows the corresponding caustic topology and source trajectory (4.2 by 4.2 Einstein angles). The caustic is computed with Caustic Finder by Schmidt, published 2008 at causticfinder.sourceforge.net.

et al. 2010), it is possible to draw a microlensing trajectory experiencing five pairs of caustic crossings for a binary lens with a mass ratio slightly smaller than one, see Fig. 10. This is a morphology that is not present in this equal-mass catalogue. Indeed, most of the new morphologies appearing in unequal-mass binary microlensing would come from the close topology. Our plots of the iso-peak regions in the (u_0, α) space are done at fixed separation s . We can follow the evolution of iso-maxima regions with a variation of s in different plots and it is easy to refine the sampling in s in order to catch all possible regions arising only in limited ranges of s . The addition of a new parameter would make the search much more complicated, as we should trace the evolution of iso-maxima regions in a two-dimensional space with the danger that tiny intersections may escape a search with a too coarse grid. New tricks are needed in order to carry out this search efficiently and without omissions. The equal-mass catalogue represents a good basis for this exploration and an already powerful map for the comprehension of microlensing of binary systems.

ACKNOWLEDGEMENTS

This publication was supported by NPRP grant NPRP-09-476-1-78 from the Qatar National Research Fund (a member of Qatar Foundation).

REFERENCES

- Albrow M. D. et al., 1999a, *Astrophysical Journal*, 522, 1022
 Albrow M. D. et al., 1999b, *Astrophysical Journal*, 522, 1011
 An J. H. et al., 2002, *Astrophysical Journal*, 572, 521
 Bennett D. P., 2010, *Astrophysical Journal*, 716, 1408
 Bennett D. P. et al., 2012, *Astrophysical Journal*, 757, 119
 Bozza V., 2001, *Astronomy & Astrophysics*, 374, 13
 Bozza V., 2010, *Monthly Notices of the Royal Astronomical Society*, 1271
 Bozza V. et al., 2012, *Monthly Notices of the Royal Astronomical Society*, 424, 902
 Cassan A., 2008, *Astronomy and Astrophysics*, 491, 587
 Cassan A., Horne K., Kains N., Tsapras Y., Browne P., 2010, *Astronomy and Astrophysics*, 515,
 Daněk K., Heyrovský D., 2015a, arxiv:1501.06519
 Daněk K., Heyrovský D., 2015b, arxiv:1501.02722
 Di Stefano R., Perna R., 1997, *Astrophysical Journal*, 488, 55
 Dominik M., 1999a, *Astronomy and Astrophysics*, 341, 943
 Dominik M., 1999b, *Astronomy and Astrophysics*, 349, 108
 Dominik M., Hirshfeld A. C., 1996, *Astronomy and Astrophysics*, 313, 841
 Einstein A., 1936, *Science*, 84, 506
 Erdl H., Schneider P., 1993, *Astronomy and Astrophysics*, 268, 453
 Gaudi B. S., Petters A. O., 2002, *Astrophysical Journal*, 574, 970
 Han C., Gaudi B. S., 2008, *Astrophysical Journal*, 689, 53
 Liebig C., 2014, PhD thesis, University of St Andrews
 Mao S., Di Stefano R., 1995, *Astrophysical Journal*, 440, 22
 Mao S., Witt H. J., An J. H., 2013, *Monthly Notices of the Royal Astronomical Society*
 Night C., Di Stefano R., Schwamb M., 2008, *Astrophysical Journal*, 686, 785
 Paczynski B., 1986, *Astrophysical Journal*, 304, 1
 Penny M. T., 2014, *Astrophysical Journal*, 790, 142
 Petters A. O., Levine H., Wambsgans J., 2001, *Progress in mathematical physics*, Vol. 21, Singularity theory and gravitational lensing. Birkhäuser
 Rhie S. H., 2002, arxiv:astro-ph/0202294v1
 Schneider P., Ehlers J., Falco E. E., 1992, *Gravitational Lenses*. Springer
 Schneider P., Weiß A., 1986, *Astronomy and Astrophysics*, 164, 237
 Skowron J. et al., 2011, *Astrophysical Journal*, 738, 87
 Skowron J., Wyrzykowski Ł., Mao S., Jaroszyński M., 2009, *Monthly Notices of the Royal Astronomical Society*, 393, 999
 Vermaak P., 2007, PhD thesis, University of Cape Town

Table 3: Morphology classes (continued).

Morphology Class	Close	Intermediate	Wide
C-F-F-F	-	-	$[A_1 b_1] D_1 [b_{2,a_2}]$
F-F-C-C	$[a_{pp1} a_{pp1}] C_{ip} C_{is} B_{i2}$	-	-
C-C-F-C	$B_{b1} C_{pp} [a_{pp1} C_{ip}] B_{i2}$	-	-
F-F-F-F-F	$[b_{b,abs1}] [a_{pp1} a_{pp1}] [a_{s1} b_1], [a_{pp1} a_{pp1}] [a_{s1} a_2] [a_{s2} b_1], [b_{b,abs1}] [a_{s1} a_2] [a_{s2} b_1]$	$[b_{b,abs1}] [a_{s1} a_2] [a_{s2} b_1], [a_{pp1} a_{pp1}] [a_{s1} b_1], [a_{pp1} a_{pp1}] [a_{s1} a_2] [a_{s2} b_1]$	-
C-F-F-F-C	$[b_{b,abs1}] [a_{pp1} a_{pp1}] [a_{s2} b_1]$	$A_1 [a_{s1} b_1] [b_{2,a_2}] A_2$	$A_1 [a_{s1} b_1] [b_{2,a_2}] A_2, A_1 [a_{pp1} b_{b1}] [b_{2,a_2}] A_2, A_1 [a_{pp1} b_{b1}] [b_{2,a_2}] A_2$
C-F-F-F-F	$B_{b1} [a_{pp1} a_{pp1}] C_{ip} [a_{s2} b_1], B_{b1} [a_{pp1} a_{pp1}] C_{ip} [a_{s2} b_1]$	-	$A_1 [a_{s1} b_1] D_1 [b_{2,a_2}] A_2, A_1 [a_{s1} b_1] D_1 [b_{2,a_2}] A_2$
C-F-F-F-F	$B_{b1} [a_{pp1} a_{pp1}] [a_{s2} b_1]$	-	$A_1 [a_{pp1} b_{b1}] [b_{2,a_2}]$
F-C-C-C-F	$[b_{b,Cbs}] [C_{ip} C_{ip}] [C_{is} b_1]$	-	$[A_1 b_1] D_1 [b_{2,a_2}] A_2$
C-F-F-C-F	$B_{b1} [a_{pp1} a_{pp1}] C_{ip} [C_{is} b_1]$	-	-
F-F-F-C-F	$[b_{b,abs1}] [a_{pp1} a_{pp1}] [C_{is} b_1]$	-	-
F-F-F-C-F	$[b_{b,abs1}] [a_{pp1} C_{ip}] [a_{s2} b_1]$	-	-
C-C-C-F-C	-	-	$[A_1 D_1] D_2 [b_{2,a_2}] A_2$
C-F-C-F-C	-	-	$A_1 [a_{pp1} D_1] [b_{2,a_2}] A_2$
C-C-F-F-C	$B_{b1} C_{pp} [a_{pp1} a_{pp2}] C_{ip} B_{i2}, B_{b1} C_{pp} [a_{pp1} a_{pp2}] C_{ip} B_{i1}$	-	-
C-C-F-F-C	$B_{b1} C_{pp} [a_{pp1} C_{ip}] C_{is} B_{i2}$	-	-
C-F-F-C-C	$B_{b1} [a_{pp1} a_{pp1}] C_{ip} C_{is} B_{i2}$	-	-
F-F-F-C-F-F	$[b_{b,abs1}] [a_{pp1} a_{pp1}] C_{ip} [a_{s2} b_1], [b_{b,abs1}] [a_{pp1} a_{pp1}] C_{ip} [a_{s1} b_1], [b_{b,abs1}] [a_{pp1} a_{pp2}] C_{ip} [a_{s2} b_1]$	-	-
C-F-F-C-F-F	$B_{b1} [a_{pp1} a_{pp1}] C_{ip} C_{is} [a_{s2} b_1], B_{b1} [a_{pp1} a_{pp1}] C_{ip} C_{is} [a_{s1} b_1]$	-	-
C-C-F-C-C	$[b_{b,abs1}] [a_{pp1} a_{pp1}] C_{ip} [C_{is} b_1]$	-	-
C-C-F-C-C	$B_{b1} C_{bs} C_{pp} [a_{pp1} C_{ip}] C_{is} B_{i2}$	-	-
F-F-F-C-C-F	$B_{b1} C_{pp} [a_{pp1} a_{pp1}] C_{ip} C_{is} B_{i2}$	-	-
C-F-F-C-C-F	$[b_{b,abs1}] C_{bs} [C_{ip} C_{ip}] [C_{is} b_1]$	-	-
C-F-F-C-C-F	$B_{b1} C_{pp} [a_{pp1} a_{pp1}] C_{ip} [C_{is} b_1]$	-	-
C-F-F-C-F-F	-	-	$A_1 [a_{pp1} D_1] D_2 [b_{2,a_2}] A_2$
C-F-F-C-F-F	-	-	$[A_1 b_1] D_1 D_2 [b_{2,a_2}] A_2$
C-F-F-C-F-F	-	-	$A_1 [a_{pp1} b_{b1}] D_1 [b_{2,a_2}] A_2, A_1 [a_{pp1} b_{b1}] D_1 [b_{2,a_2}] A_2$
C-F-F-F-F-F	$B_{b1} [a_{pp1} a_{pp1}] [a_{pp1} a_{pp2}] [a_{s2} b_1]$	-	$A_1 [a_{pp1} b_{b1}] [b_{2,a_2}]$
F-F-F-F-F-F	$[b_{b,abs1}] C_{pp} [a_{pp1} a_{pp1}] C_{ip} [a_{s1} b_1], [b_{b,abs1}] C_{pp} [a_{pp1} a_{pp2}] C_{ip} [a_{s2} b_1], [b_{b,abs1}] C_{pp} [a_{pp1} a_{pp1}] C_{ip} [a_{s2} b_1]$	-	-
F-F-F-F-F-F	$[b_{b,abs1}] C_{bs} [C_{is} C_{ip}] C_{is} [a_{s2} b_1]$	-	-
F-F-F-F-F-F	$[b_{b,abs1}] C_{bs} [a_{pp1} C_{ip}] C_{is} [a_{s2} b_1], [b_{b,abs1}] C_{pp} [a_{pp1} C_{ip}] C_{is} [a_{s1} b_1]$	-	-
F-F-F-F-F-F	$[b_{b,abs1}] C_{bs} C_{pp} [a_{pp1} C_{ip}] [C_{is} b_1]$	-	-
F-F-F-F-F-F	$[b_{b,abs1}] C_{bs} [a_{pp1} a_{pp1}] C_{ip} [C_{is} b_1]$	-	-
F-F-F-F-F-F	$[b_{b,abs1}] [a_{pp1} a_{pp1}] C_{ip} C_{is} [a_{s2} b_1], [b_{b,abs1}] [a_{pp1} a_{pp1}] C_{ip} C_{is} [a_{s1} b_1]$	-	-

VI

VII

VIII

Continued on next page.

Table 3: Morphology classes (continued).

Morphology Class	Close	Intermediate	Wide
$\tilde{C} \tilde{C} F \tilde{C} \tilde{C}$	$B_{b_1} C_{b_s} C_{cp} [a_{b_1} a_{p_2}] C_{cp} C_{s_1} B_{b_2} B_{b_1} C_{b_s} C_{cp} [a_{b_1} a_{p_1}] C_{cp} C_{s_1} B_{b_1}$	-	-
$\tilde{C} \tilde{C} F \tilde{C} F F$	$B_{b_1} C_{b_s} C_{cp} [a_{b_1} a_{p_1}] C_{cp} C_{s_1} [a_{s_2} b_1] B_{b_1} C_{b_s} C_{cp} [a_{b_1} a_{p_1}] C_{cp} C_{s_1} [a_{s_1} b_1]$	-	-
$\tilde{C} \tilde{C} F \tilde{C} C F$	$B_{b_1} C_{b_s} C_{cp} [a_{b_1} a_{p_1}] C_{cp} [C_{s_1} b_1]$	-	-
$\tilde{C} F \tilde{C} F F \tilde{C}$	$A_1 [a_{b_1} b_{b_1}] D_1 D_2 [b_{b_2} a_{a_2}] A_2$	-	-
$F F \tilde{C} \tilde{C} F C \tilde{C} F F$	$[b_{b_1} a_{b_s}] C_{b_s} C_{cp} [a_{b_1} a_{p_1}] C_{cp} [C_{s_1} [a_{s_2} b_1]]$	-	-
$F F \tilde{C} \tilde{C} F F \tilde{C} C F$	$[b_{b_1} a_{b_s}] C_{b_s} C_{cp} [a_{b_1} a_{p_1}] C_{cp} [C_{s_1} b_1]$	-	-
$\tilde{C} \tilde{C} \tilde{C} F F \tilde{C} F F$	$B_{b_1} C_{b_s} C_{cp} [a_{b_1} a_{p_1}] C_{cp} C_{s_1} [a_{s_2} b_1] B_{b_1} C_{b_s} C_{cp} [a_{b_1} a_{p_1}] C_{cp} C_{s_1} [a_{s_1} b_1]$	-	-
$F F \tilde{C} F F \tilde{C} F F$	$[b_{b_1} a_{b_s}] C_{b_s} C_{cp} [a_{b_1} a_{p_1}] C_{cp} C_{s_1} [a_{s_2} b_1] [b_{b_1} a_{b_s}] C_{b_s} C_{cp} [a_{b_1} a_{p_1}] C_{cp} C_{s_1} [a_{s_1} b_1]$	-	-
$F F \tilde{C} \tilde{C} F F \tilde{C} F F$	$[b_{b_1} a_{b_s}] C_{b_s} C_{cp} [a_{b_1} a_{p_1}] C_{cp} C_{s_1} [a_{s_2} b_1] [b_{b_1} a_{b_s}] C_{b_s} C_{cp} [a_{b_1} a_{p_1}] C_{cp} C_{s_1} [a_{s_1} b_1]$	-	-
X			

Figure 11. Morphology class sample light curves, cf. Table 3, all to same scale (magnification 1 to 50, with dotted line at 10). Scale and ranges as in Fig. 10.

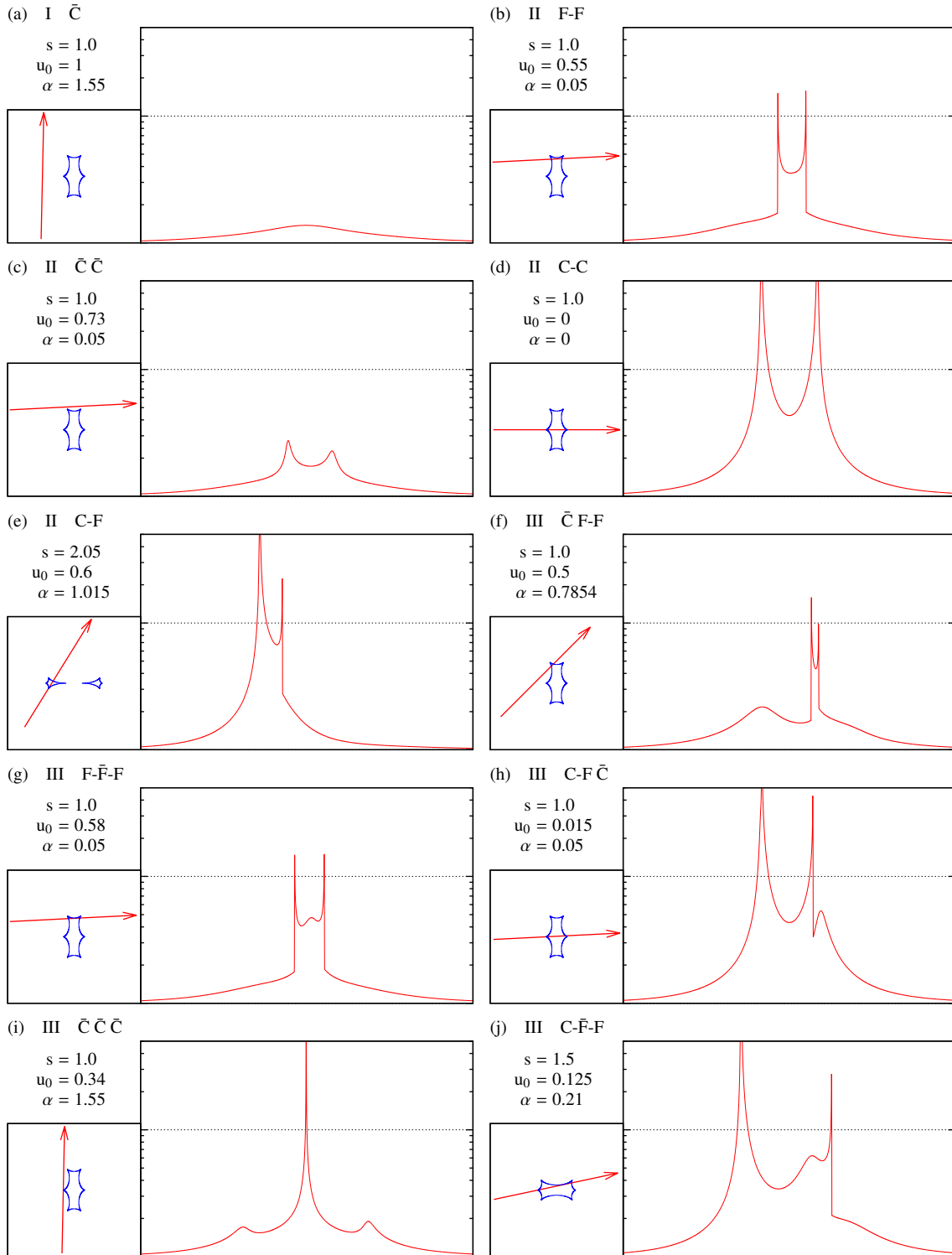


Figure 12. Morphology class sample light curves. (Continued.)

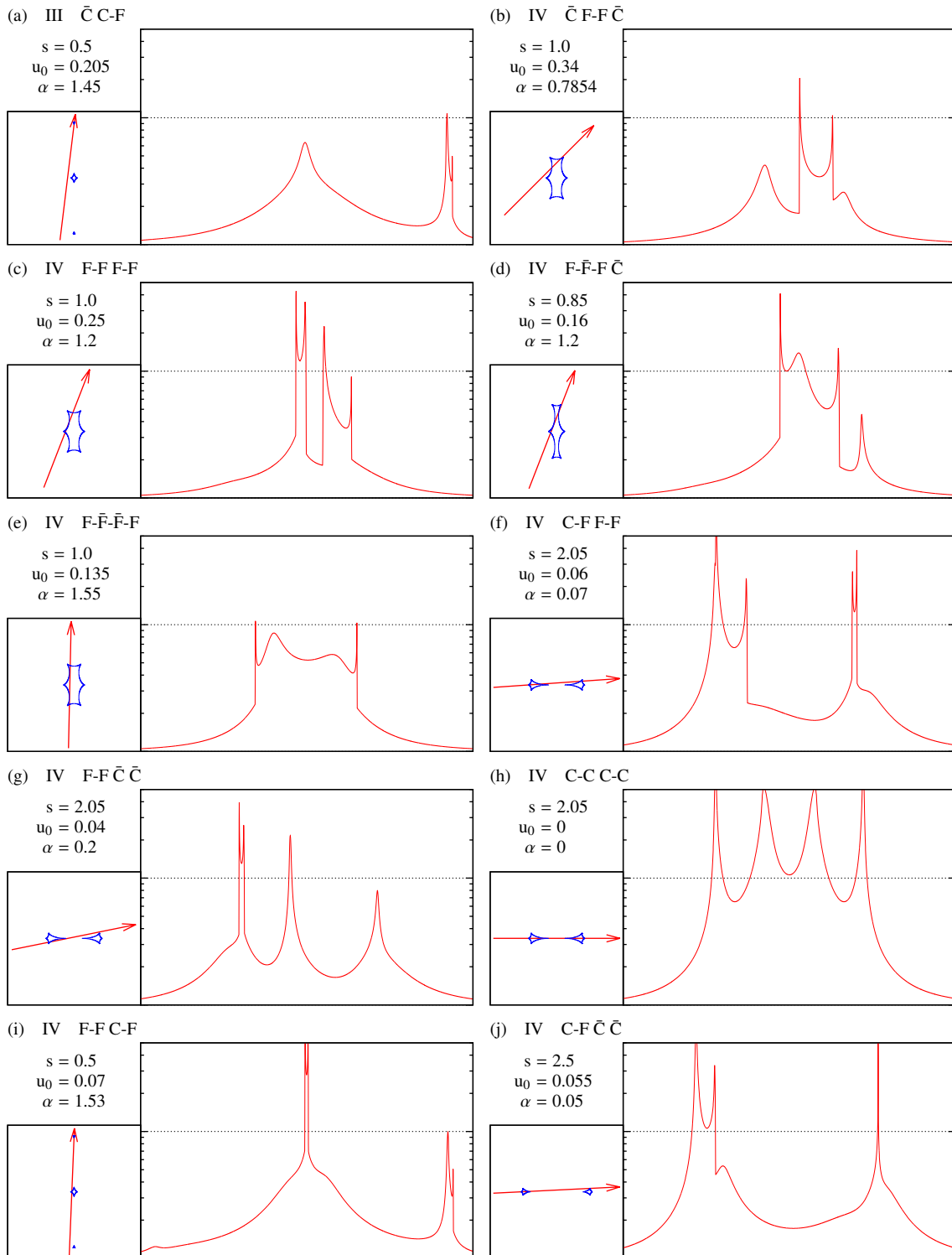


Figure 13. Morphology class sample light curves. (Continued.)

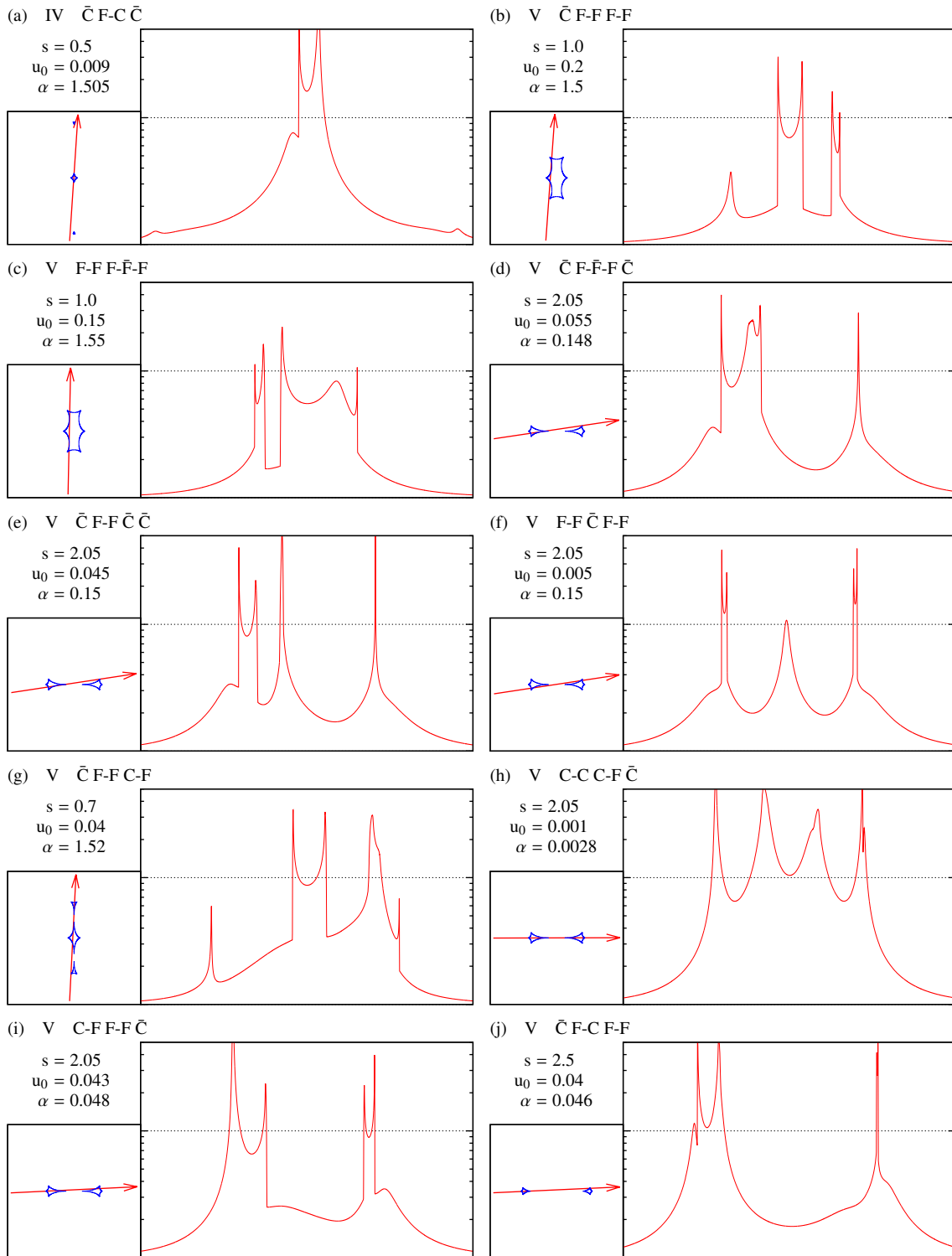


Figure 14. Morphology class sample light curves. (Continued.)

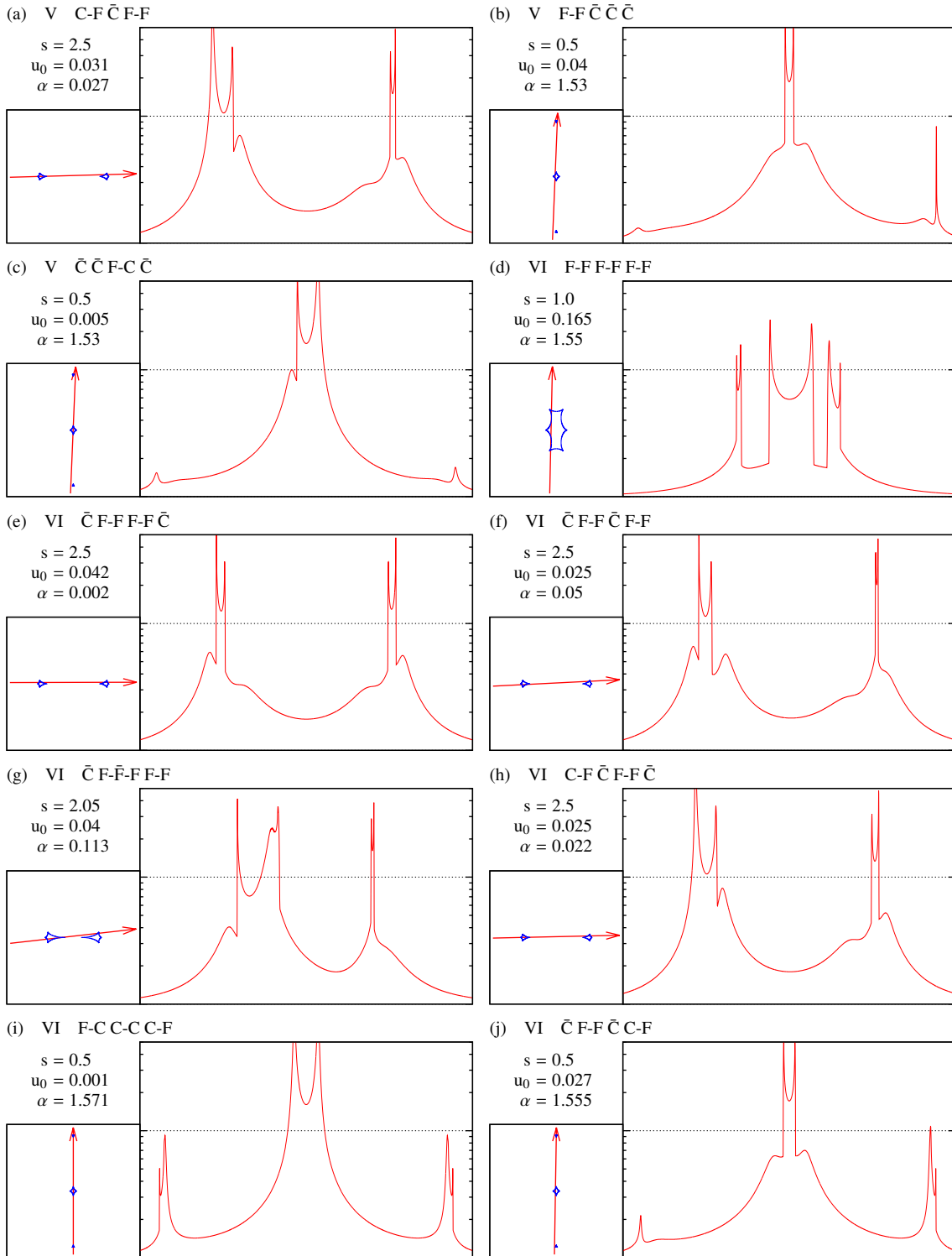


Figure 15. Morphology class sample light curves. (Continued.)

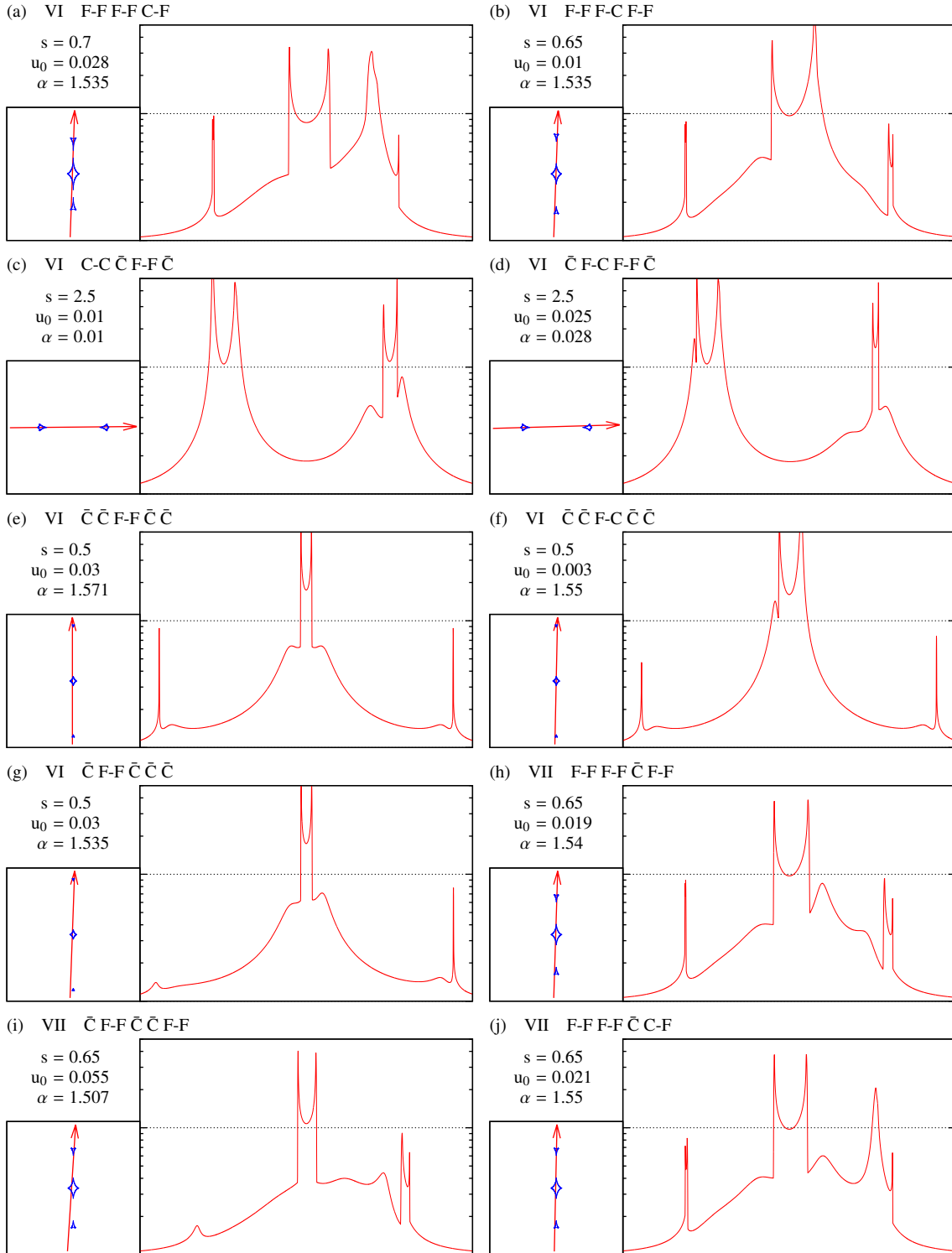


Figure 16. Morphology class sample light curves. (Continued.)

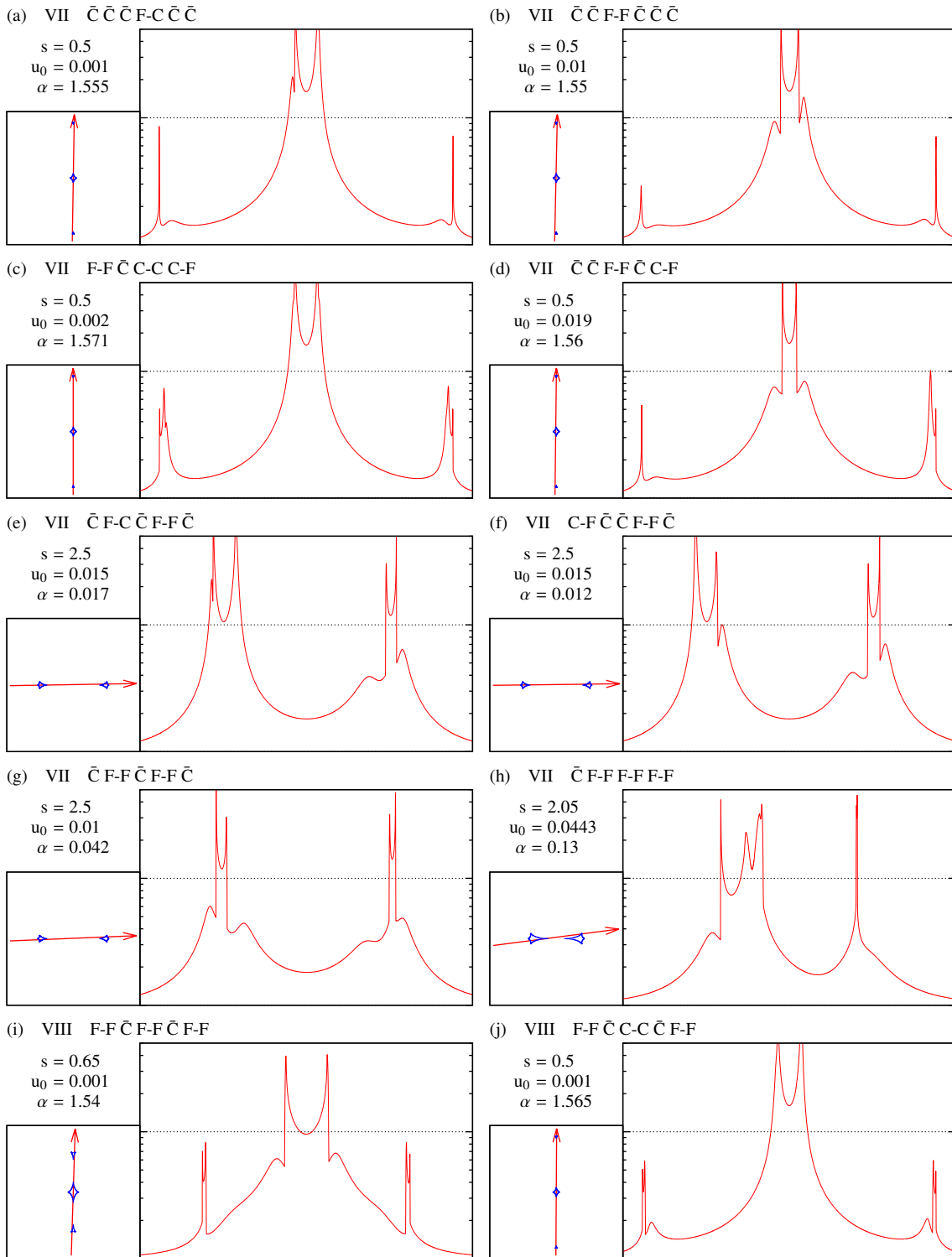


Figure 17. Morphology class sample light curves. (Continued.)

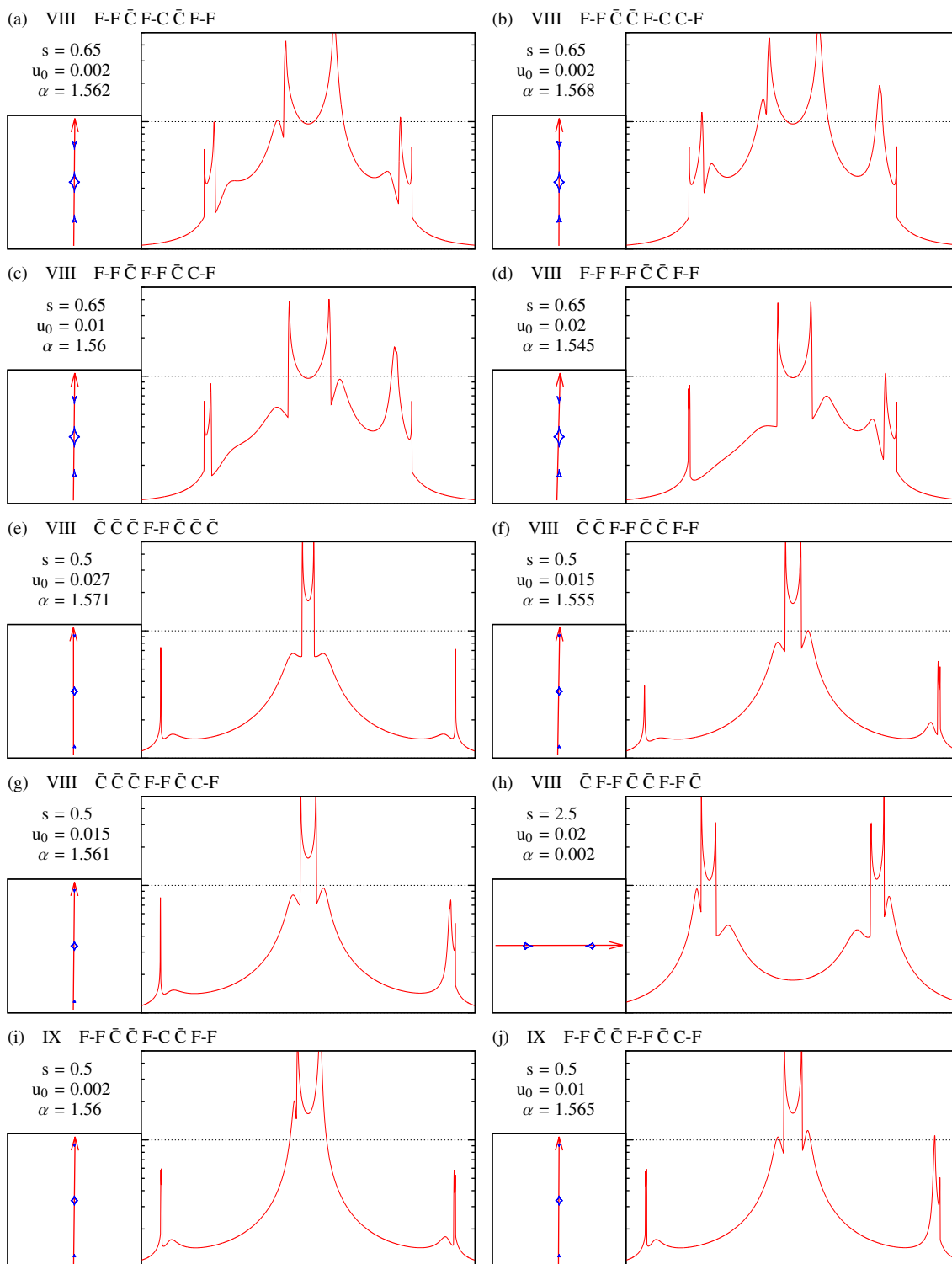


Figure 18. Morphology class sample light curves. (Continued.)

